53BP1 Regulates DSB Repair Using Rif1 to Control 5′ End Resection

Michal Zimmermann *et al.*

Science **339**, 700 (2013);
DOI: 10.1126/science.1231573

53BP1 Regulates DSB Repair Using Rif1 to Control 5′ End Resection

Michal Zimmermann,[1,2] Francisca Lottersberger,[1] Sara B. Buonomo,[3] Agnel Sfeir,[1]* Titia de Lange[1]†

The choice between double-strand break (DSB) repair by either homology-directed repair (HDR) or nonhomologous end joining (NHEJ) is tightly regulated. Defects in this regulation can induce genome instability and cancer. 53BP1 is critical for the control of DSB repair, promoting NHEJ, and inhibiting the 5′ end resection needed for HDR. Using dysfunctional telomeres and genome-wide DSBs, we identify Rif1 as the main factor used by 53BP1 to impair 5′ end resection. Rif1 inhibits resection involving CtIP, BLM, and Exo1; limits accumulation of BRCA1/BARD1 complexes at sites of DNA damage; and defines one of the mechanisms by which 53BP1 causes chromosomal abnormalities in Brca1-deficient cells. These data establish Rif1 as an important contributor to the control of DSB repair by 53BP1.

The DNA damage response protein 53BP1 can influence the type of DNA repair at double-strand breaks (DSBs) (*1*) as seen in immunoglobulin gene rearrangements (*2*–*4*) and in the fusion of telomeres rendered dysfunctional through the removal of the shelterin protein TRF2 (*5*), where 53BP1 enhances the mobility of damaged telomeres, thus potentially promoting the chance of telomere-telomere encounters. In Brca1-deficient cells, 53BP1 enhances aberrant nonhomologous end joining (NHEJ) events that create lethal radial chromosomes in response to poly(ADP-ribose) polymerase PARP1 inhibitors (PARPi) (*6*). In this setting, 53BP1 may favor NHEJ-mediated misrejoining by blocking the DSB resection needed for homology-directed repair (HDR) (*6*, *7*). 53BP1 was shown to impede 5′ end resection at dysfunctional telomeres lacking all shelterin proteins and, similarly, telomeres lacking only TRF2 show evidence of 53BP1-dependent protection from resection (*5*, *8*). Based on the finding that an allele of 53BP1 (53BP1^{28A}) lacking all potential ataxia telangiectasia mutated (ATM)/ATM and Rad3-related (ATR) kinase S/TQ target sites did not support immunoglobulin class switch recombination (CSR) and failed to generate radial chromosomes in Brca1-deficient cells (*7*), it appears that these functions of 53BP1 involve interacting partner(s) modulated by the S/TQ sites. One candidate 53BP1-interacting factor is Rif1, which localizes to DSBs and dysfunctional telomeres, in a manner that is dependent on ATM signaling (*9*–*11*). Rif1 was originally identified as part of the telomeric complex in budding yeast (*12*) and was recently shown to inhibit resection at yeast telomeres (*13*, *14*). In contrast, mammalian Rif1 has no known function at functional telomeres but contributes to the intra–S phase checkpoint, facilitates recovery from replication stress, and affects replication timing (*10*, *15*–*17*).

We introduced 53BP1^{28A} and other 53BP1 mutant alleles (*7*) into immortalized TRF2$^{F/-}$53BP1$^{-/-}$ mouse embryo fibroblasts (MEFs) and induced telomere dysfunction by deletion of TRF2 (Fig. 1, A and B). The results showed that the S/TQ sites were required for the accumulation of Rif1 at deprotected telomeres, whereas the GAR, BRCT, and oligomerization domains of 53BP1 were not

[1]Laboratory for Cell Biology and Genetics, Rockefeller University, New York, NY 10065, USA. [2]Central European Institute of Technology and Faculty of Science, Masaryk University, Brno, Czech Republic. [3]European Molecular Biology Laboratory, Mouse Biology Unit, Monterotondo, Italy.

*Present address: Developmental Genetics Program and Department of Cell Biology, Skirball Institute, New York University School of Medicine, New York, NY 10016, USA.
†To whom correspondence should be addressed. E-mail: delange@mail.rockefeller.edu

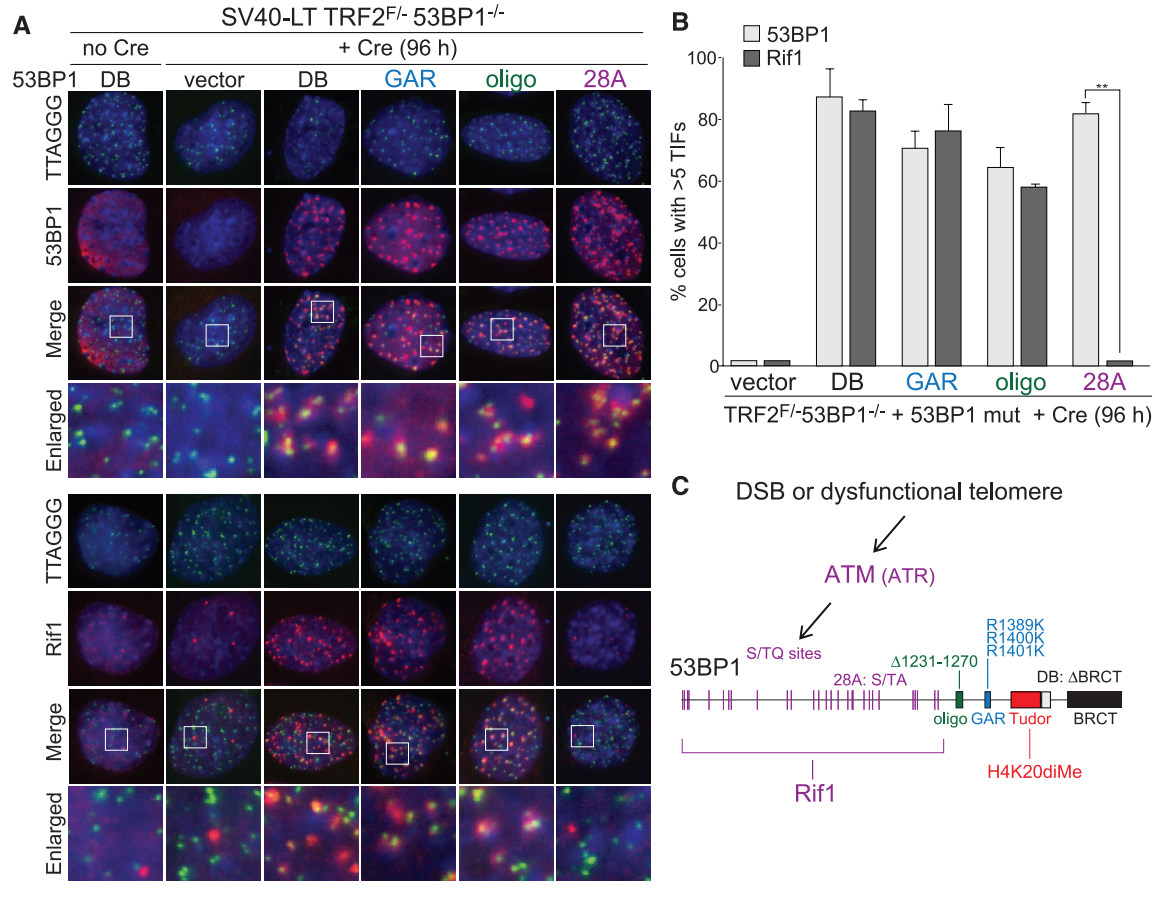

Fig. 1. Rif1 recruitment requires the S/TQ ATM/ATR target sites of 53BP1. (**A**) Detection of 53BP1 and Rif1 at dysfunctional telomeres in Cre-treated SV40 large T antigen (SV40-LT) immortalized TRF2$^{F/-}$53BP1$^{-/-}$ MEFs expressing 53BP1 mutant alleles [shown in (C)]. Indirect immunofluorescence (IF) for 53BP1 and Rif1 (red) was combined with telomeric TTAGGG fluorescence in situ hybridization (FISH) (green). Blue: 4′,6-diamidino-2-phenylindole DNA stain. (**B**) Quantification of 53BP1 and Rif1 telomere dysfunction–induced foci (TIFs) (*21*) detected as in (A). Data represent means of three experiments ±SDs (≥70 cells per experiment). **, $P < 0.05$ (two-tailed paired Student's *t* test). (**C**) Schematic of the 53BP1 mutant alleles and the role of the N-terminal S/TQ sites in the recruitment of Rif1.

(Fig. 1, A to C, and fig. S1). The functional importance of the Rif1-53BP1 interaction was addressed using a telomere-based assay system that previously uncovered the role of 53BP1 in stimulating telomeric NHEJ and protecting telomere ends from 5′ resection (*5*, *8*). Using TRF2/Rif1 conditional double-knockout MEFs, we documented a significant reduction in the incidence and rate of telomere fusions in cells lacking Rif1 (Fig. 2, A to C, and fig. S2A). This reduced NHEJ rate was not due to changes in cell cycle progression or diminished activation of the ATM kinase pathway by the deprotected telomeres (fig. S2, B to G).

As 53BP1 increases the mobility of dysfunctional telomeres, we determined whether Rif1 contributes to this aspect of 53BP1 by live-cell imaging of mCherry fused to the 53BP1 Tudor domain, which targets this marker to dysfunctional telomeres (fig. S2H). As expected, traces of the mCherry marker demonstrated that 53BP1 deficiency reduced the mobility of dysfunctional telomeres (Fig. 2D). In contrast, absence of Rif1 did not affect the mobility of the deprotected telomeres. Thus, Rif1 is not required for the 53BP1-dependent increase in the mobility of dysfunctional telomeres.

We next determined whether Rif1 contributes to the inhibition of 5′ end resection by 53BP1. When TRF2 is deleted from cells lacking 53BP1, there is a 2- to 3-fold increase in the telomeric 3′ overhang signal (*5*) which can be detected based on annealing a telomeric oligonucleotide to native telomeric DNA (Fig. 3). As expected, deletion of TRF2 resulted in the removal of the overhangs concomitant telomere fusion, whereas the overhang signal increased 3-fold when TRF2 was deleted from 53BP1-deficient cells in which telomeric NHEJ is rare and 5′ end resection is uninhibited (Fig. 3, A and B). Deletion of TRF2 from Rif1-deficient cells also resulted in an increase in the overhang signal (Fig. 3B). However, the increase was less compared to that observed in the 53BP1-deficient cells. Because the difference might be due to the lower rate of telomere fusions in the 53BP1-deficient setting, we generated immortalized $TRF2^{F/F}Lig4^{-/-}Rif1^{F/F}$ cells, which, owing to the absence of DNA ligase IV, have the same low telomere fusions rates as $TRF2^{F/-}53BP1^{-/-}$ cells (*5*). When NHEJ was blocked, the telomeric overhang increase in the Rif1-deficient cells was the same as that which occurred in the 53BP1-deficient cells (Fig. 3, C and D). The increase in overhang signal was demonstrably due to 3′ terminal sequences because the signal was removed by digestion with the *Escherichia coli* 3′ exonuclease ExoI (fig. S3A). These data suggest that Rif1 is the main factor acting downstream of 53BP1 to inhibit the resection at telomeres that lack TRF2 protection.

At telomeres that are deprived of both TRF1 and TRF2 and therefore lack all shelterin proteins, 53BP1 blocks extensive 5′ end resection that involves CtIP, BLM, and Exo1 (*8*). To test the ability of Rif1 to inhibit resection at such shelterin-free telomeres, we generated immortalized $TRF1^{F/F}TRF2^{F/F}Rif1^{F/F}$ MEFs. As expected, deletion of TRF1 and TRF2 resulted in frequent telomere fusions and nearly complete loss of the telomeric overhang signal when Rif1 was present (Fig. 3, E and F). When Rif1 was codeleted with TRF1 and TRF2, telomere fusions were also frequent, resulting in most telomeric restriction fragments shifting to a higher molecular weight (Fig. 3E). However, the telomeres that had not fused at the time point analyzed showed a notable increase in overhang signal (Fig. 3, E and F). This increase in the signal was diminished when cells were treated with short hairpin RNAs (shRNAs) against CtIP, BLM, or Exo1 (Fig. 3, G and H, and fig. S3, B and C). Thus, like 53BP1, Rif1 inhibits 5′ end resection that involves CtIP, BLM, and Exo1.

We next asked whether Rif1 affects resection at zeocin-induced DSBs by monitoring the formation of replication protein A (RPA) foci (Fig. 4A and fig. S4A). The absence of either Rif1, 53BP1, or both did not affect zeocin-induced γ-H2AX foci or the basal level of cells containing γ-H2AX foci, which likely represent replicating cells (Fig. 4, A and B). However, in zeocin-treated cells, the absence of either Rif1 or 53BP1 resulted in a significant increase in γ-H2AX foci that colocalized with RPA (Fig. 4, A and C). When either 53BP1 or Rif1 were absent, there also was a significant increase in γ-H2AX foci containing RPA in cells not treated with zeocin, presumably reflecting a higher level of resection at stalled replication forks (Fig. 4, A and C). Examination of the RPA/γ-H2AX foci in zeocin-treated

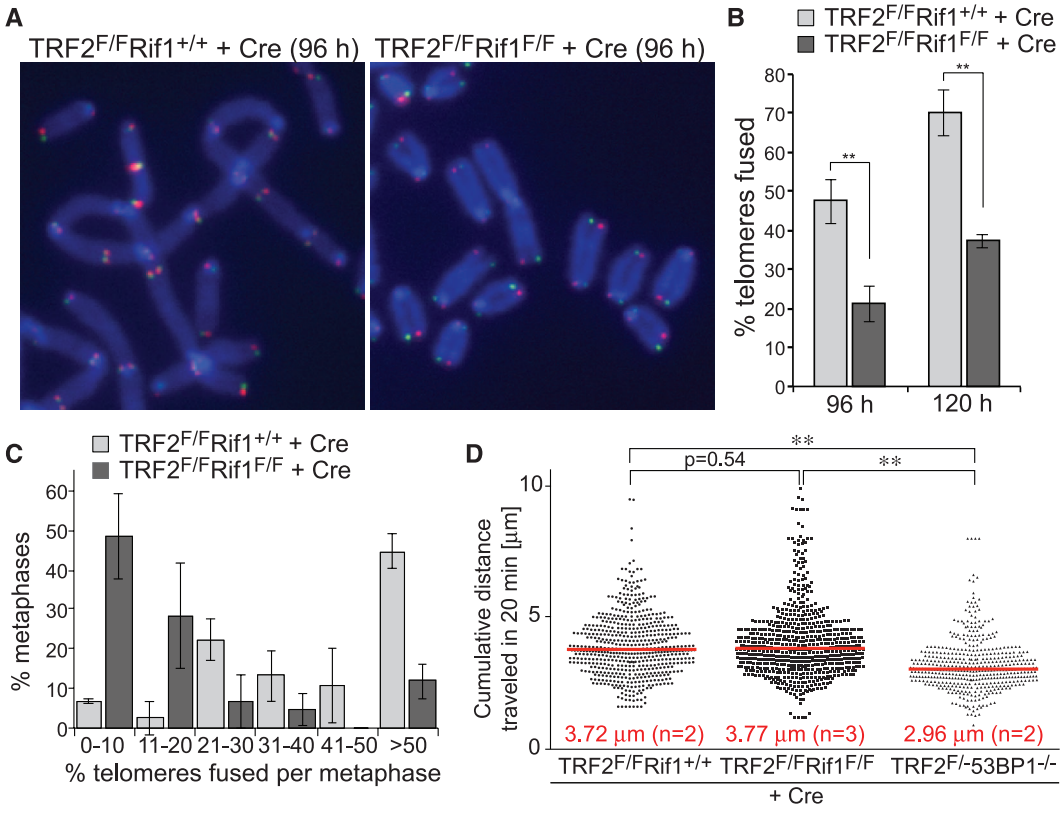

Fig. 2. Rif1 promotes telomeric NHEJ without affecting telomere mobility. (**A**) Metaphase chromosomes of Cre-treated SV40-LT immortalized $TRF2^{F/F}Rif1^{+/+}$ and $TRF2^{F/F}Rif1^{F/F}$ MEFs showing NHEJ-mediated telomere fusions detected by *chromosome orientation* FISH. Telomeres synthesized by leading-end DNA synthesis are in red; lagging-end telomeres are in green. (**B**) Quantification of telomere fusions as determined in (A) at 96 and 120 hours after Cre. Data represent means of three independent experiments ±SDs (>3000 telomeres per experiment). **, $P < 0.01$ based on two-tailed paired Student's *t* test. (**C**) Distributions of telomere fusions per metaphase at 96 hours after Cre for experiments shown in (B). (**D**) Distribution of cumulative distances traveled by mCherry-$53BP1^{1220\text{-}1711}$ foci in the indicated cell lines. Red lines represent medians. **, $P < 0.0001$ (two-tailed Mann-Whitney test).

Rif1/53BP1 double-knockout cells indicated that Rif1 and 53BP1 are epistatic in this regard because the induction of RPA/γ-H2AX foci in absence of 53BP1 was the same as in Rif1-deficient cells and the absence of both Rif1 and 53BP1 did not further increase the response (Fig. 4C). The simplest interpretation of these data is that Rif1 is the main factor acting downstream of 53BP1 to block 5′ end resection at the zeocin-induced DSBs.

Because the 53BP1/Rif1 control affects CtIP, which is thought to be delivered by a complex containing BRCA1 (*18*–*20*), we also determined whether 53BP1 and Rif1 had an effect on the presence of the BRCA1 at zeocin-induced DSBs. Using an antibody to the constitutive BRCA1 partner BARD1, we found that absence of Rif1 or 53BP1 resulted in a significant increase in the accumulation of BRCA1 complexes at zeocin-induced DSBs (Fig. 4, E and F). Consistent with the data above, Rif1 and 53BP1 were again epistatic in this regard. The absence of 53BP1 resulted in the same phenotype as absence of Rif1, and the double knockout did not show an additional increase in the incidence of BARD1 foci (Fig. 4, E and F). The absence of Rif1 also resulted in an increase in the presence of BARD1 at dysfunctional telomeres (fig. S4, B to D).

Because 53BP1 mediates the formation of misrejoined and radial chromosomes in PARPi-treated Brca1-deficient cells, we asked to what extent Rif1 is responsible for this effect. Cells lacking Rif1, 53BP1, or both were treated with a BRCA1 shRNA and the PARP inhibitor, and misrejoined chromosomes were quantified (Fig. 4, G and H). The data show the previously documented decrease in the frequency of chromosome misrejoining when 53BP1 is absent. Interestingly, absence of Rif1 also lowers the frequency of chromosome misrejoining, but the effect is significantly less than for 53BP1. Thus, the formation of misrejoined chromosomes in PARPi-treated Brca1-deficient cells is due to two distinct attributes of 53BP1, one of which requires Rif1 function.

These data identify Rif1 as the major factor acting downstream of 53BP1 in the control of 5′

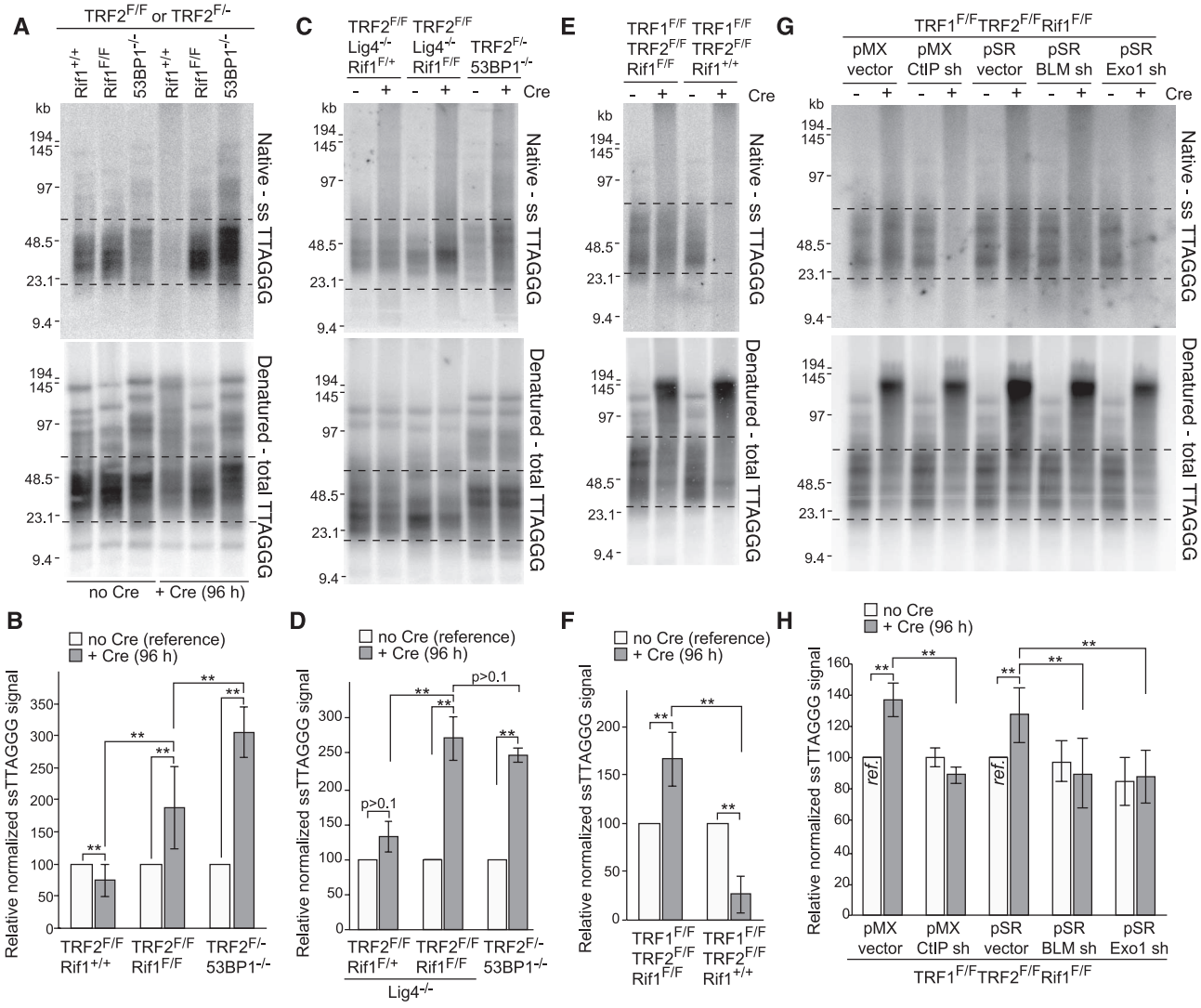

Fig. 3. Rif1 blocks 5′ end resection at dysfunctional telomeres. (**A**) Telomeric overhang assays on TRF2$^{F/F}$Rif1$^{+/+}$, TRF2$^{F/F}$Rif1$^{F/F}$ and TRF2$^{F/-}$53BP1$^{-/-}$ MEFs. Native in-gel hybridization of MboI/AluI digested DNA with end-labeled $[AACCCT]_4$ (top) and re-hybridization with the same probe after denaturation in situ (bottom). Dashed lines represent the bulk of free (unfused) telomeres used for quantification. (**B**) Quantification of overhang assays as in (A). Overhang signals in no Cre samples was set at 100%. (**C** and **D**) Overhang assays on TRF2$^{F/F}$Rif1$^{F/+}$Lig4$^{-/-}$, TRF2$^{F/F}$Rif1$^{F/F}$Lig4$^{-/-}$, and TRF2$^{F/-}$53BP1$^{-/-}$ MEFs and quantification as in (B). (**E** and **F**) Overhang assays on TRF1$^{F/F}$TRF2$^{F/F}$Rif1$^{+/+}$ and TRF1$^{F/F}$TRF2$^{F/F}$Rif1$^{F/F}$ MEFs and quantification. (**G** and **H**) Overhang assays to measure dependency on CtIP, BLM, and Exo1 and quantification. Cells infected with either pMX or pSR with or without the indicated shRNAs and treated with Cre for 96 hours. Samples with empty vectors and no Cre (*ref.*) were used as references. Data in [(B), (D), (F), and (H)] represent means of ≥3 experiments ±SDs. **, $P < 0.05$ (two-tailed paired Student's *t* test). MEFs are SV40-LT immortalized.

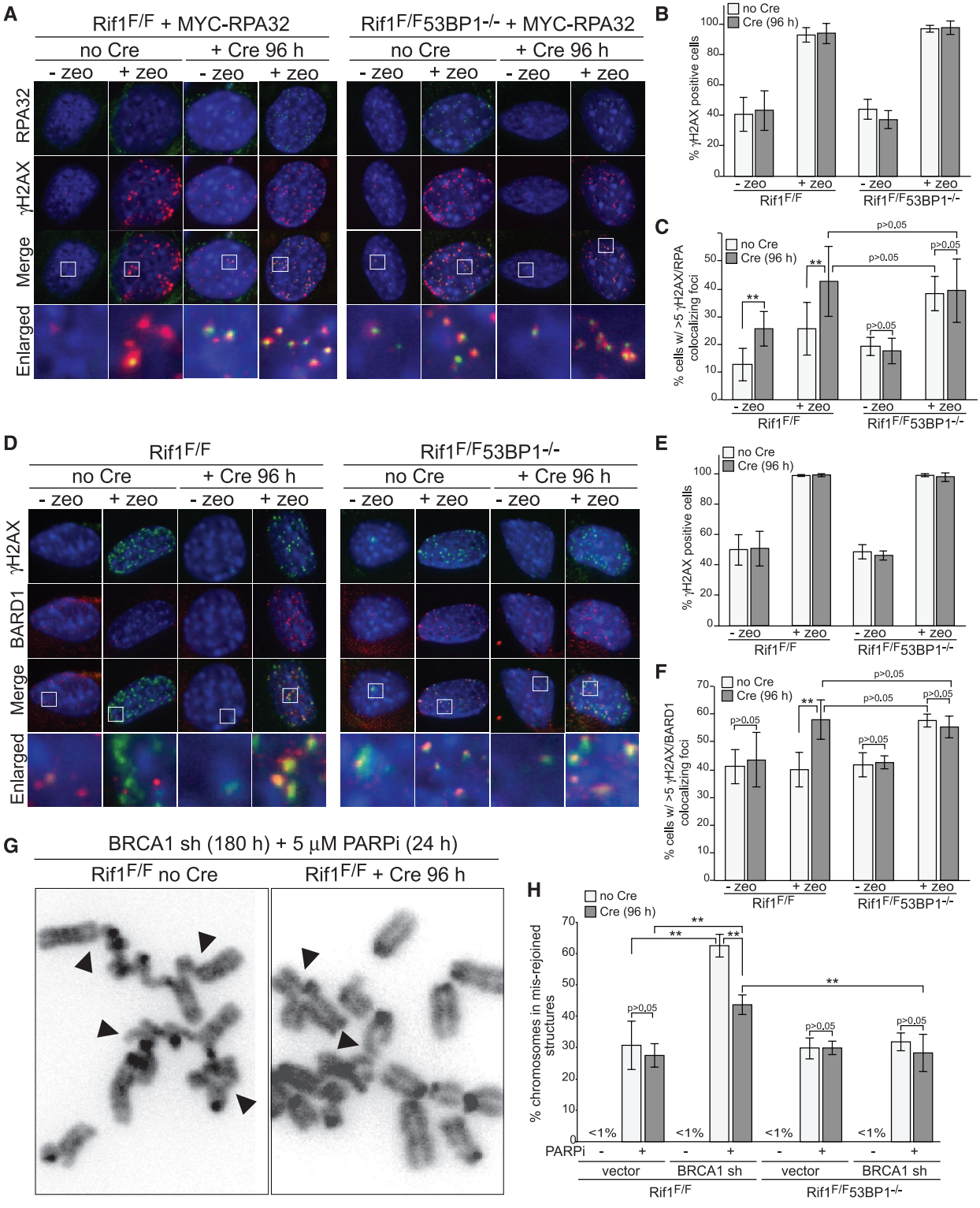

Fig. 4. Rif1 inhibits resection at DSBs and promotes radial formation. (**A**) IF for γ-H2AX (red) and MYC-RPA32 (green) in Cre-treated SV40-LT immortalized Rif1$^{F/F}$ and Rif1$^{F/F}$53BP1$^{-/-}$ cells expressing MYC-RPA32 treated with zeocin (100 μg/ml, for 1 hour; 2 hours before analysis). (**B**) Percentage of γ-H2AX positive cells in experiments as in (A). (**C**) Percentage of cells [as in (A)] scored positive when containing at least five γ-H2AX foci colocalizing with RPA. (**D**) IF for γH2AX (green) and BARD1 (red) in Rif1$^{F/F}$ and Rif1$^{F/F}$53BP1$^{-/-}$ MEFs. Cells and treatment as in (A). (**E**) Percentage of γ-H2AX-positive cells in experiments in (D). (**F**) Percentage of cells in (D) containing >5 BARD1/γ-H2AX colocalizing foci. (**G**) Examples of misrejoined and radial chromosomes (arrowheads) in BRCA1sh/PARPi-treated Rif1$^{F/F}$ cells with or without Cre. (**H**) Percentages of chromosomes that are misrejoined in the indicated genotypes and treatments. Data in (B), (C), (E), (F), and (H) are means of three to five experiments ±SDs. **, $P < 0.05$ (two-tailed paired Student's *t* test).

end resection. In contrast, Rif1 does not appear to be required for the ability of 53BP1 to promote an increase in the mobility of dysfunctional telomeres. The intermediate effect of Rif1 on the fusion of dysfunctional telomeres can be explained based on these two observations. The increased resection of dysfunctional telomeres in absence of Rif1 is likely to be responsible for the mild inhibition of NHEJ. However, in the absence of 53BP1, the effect of increased resection is combined with a defect in the induction of the mobility of the dysfunctional telomeres, resulting in a more severe blockade to NHEJ. Similarly, we propose that Rif1 deletion leads to partial rescue of chromosome misrejoining in PARPi/BRCA1 shRNA-treated cells because the control of 5′ end resection is only one of multiple mechanisms by which 53BP1 acts. One possibility is that the other mechanism used by 53BP1 in this context, similar to what happens at dysfunctional telomeres, involves the induction of DSB mobility that increases the chance that DSB misrejoining occurs.

References and Notes

1. A. T. Noon, A. A. Goodarzi, *DNA Repair* **10**, 1071 (2011).
2. I. M. Ward, K. Minn, J. van Deursen, J. Chen, *Mol. Cell. Biol.* **23**, 2556 (2003).
3. J. C. Morales *et al.*, *J. Biol. Chem.* **278**, 14971 (2003).
4. S. Difilippantonio *et al.*, *Nature* **456**, 529 (2008).
5. N. Dimitrova, Y. C. Chen, D. L. Spector, T. de Lange, *Nature* **456**, 524 (2008).
6. S. F. Bunting *et al.*, *Cell* **141**, 243 (2010).
7. A. Bothmer *et al.*, *Mol. Cell* **42**, 319 (2011).
8. A. Sfeir, T. de Lange, *Science* **336**, 593 (2012).
9. L. Xu, E. H. Blackburn, *J. Cell Biol.* **167**, 819 (2004).
10. J. Silverman, H. Takai, S. B. Buonomo, F. Eisenhaber, T. de Lange, *Genes Dev.* **18**, 2108 (2004).
11. M. S. Huen *et al.*, *Mol. Cell* **37**, 854 (2010).
12. C. F. Hardy, L. Sussel, D. Shore, *Genes Dev.* **6**, 801 (1992).
13. S. Anbalagan, D. Bonetti, G. Lucchini, M. P. Longhese, *PLoS Genet.* **7**, e1002024 (2011).
14. D. Bonetti *et al.*, *PLoS Genet.* **6**, e1000966 (2010).
15. S. B. Buonomo, Y. Wu, D. Ferguson, T. de Lange, *J. Cell Biol.* **187**, 385 (2009).
16. D. Cornacchia *et al.*, *EMBO J.* **31**, 3678 (2012).
17. S. Yamazaki *et al.*, *EMBO J.* **31**, 3667 (2012).
18. A. A. Sartori *et al.*, *Nature* **450**, 509 (2007).
19. X. Yu, L. C. Wu, A. M. Bowcock, A. Aronheim, R. Baer, *J. Biol. Chem.* **273**, 25388 (1998).
20. A. K. Wong *et al.*, *Oncogene* **17**, 2279 (1998).
21. H. Takai, A. Smogorzewska, T. de Lange, *Curr. Biol.* **13**, 1549 (2003).

Acknowledgments: We thank D. White for expert mouse husbandry and M. Nussenzweig for providing mutant 53BP1 constructs. M.Z. was supported by a Brno Ph.D. talent fellowship and by a grant from the Czech Science Foundation to Ctirad Hofr (P205/12/0550) (see supplementary materials for detailed acknowledgement). This work was supported by a grant from the Breast Cancer Research Foundation to T.d.L. T.d.L. is an American Cancer Society Research Professor.

Supplementary Materials

www.sciencemag.org/cgi/content/full/science.1231573/DC1
Materials and Methods
Figs. S1 to S4
References (*22*–*28*)

16 October 2012; accepted 14 December 2012
Published online 10 January 2013;
10.1126/science.1231573

Regulation of Flowering by Trehalose-6-Phosphate Signaling in *Arabidopsis thaliana*

Vanessa Wahl,[1]* Jathish Ponnu,[2] Armin Schlereth,[1] Stéphanie Arrivault,[1] Tobias Langenecker,[2] Annika Franke,[1] Regina Feil,[1] John E. Lunn,[1] Mark Stitt,[1] Markus Schmid[2]*

The timing of the induction of flowering determines to a large extent the reproductive success of plants. Plants integrate diverse environmental and endogenous signals to ensure the timely transition from vegetative growth to flowering. Carbohydrates are thought to play a crucial role in the regulation of flowering, and trehalose-6-phosphate (T6P) has been suggested to function as a proxy for carbohydrate status in plants. The loss of *TREHALOSE-6-PHOSPHATE SYNTHASE 1* (*TPS1*) causes *Arabidopsis thaliana* to flower extremely late, even under otherwise inductive environmental conditions. This suggests that *TPS1* is required for the timely initiation of flowering. We show that the T6P pathway affects flowering both in the leaves and at the shoot meristem, and integrate *TPS1* into the existing genetic framework of flowering-time control.

The transition from vegetative to reproductive development is an important phase change in a plant's life. When timed correctly, the transition helps to ensure reproductive success and therefore has adaptive value. For this reason, plants have evolved an intricate genetic network that controls the onset of flowering in response to environmental and endogenous signals such as day length, temperature, hormonal status, and carbohydrate availability (*1*). Day length is perceived in the leaves, where a sufficiently long day (i.e., an inductive photoperiod) leads to induction of the *FLOWERING LOCUS T* (*FT*) gene (*2*–*7*). The FT protein functions as a long-distance signal (florigen) that is transported to the shoot meristem, where it interacts with the bZIP transcription factor FD and triggers the formation of flowers (*8*–*11*).

In contrast to the detailed understanding of the photoperiod pathway, relatively little is known about the contribution of carbohydrates to the regulation of flowering (*12*). Mutations in genes of key enzymes in sugar and starch metabolism such as *HEXOKINASE1* (*HXK1*) and *PHOSPHOGLUCOMUTASE1* (*PGM1*) have been shown to affect various aspects of development, including flowering (*13*). A particularly striking example in this respect is TREHALOSE-6-PHOSPHATE SYNTHASE 1 (TPS1), which catalyzes the formation of trehalose-6-phosphate (T6P) from glucose-6-phosphate and uridine diphosphate (UDP)–glucose (*13*, *14*). T6P, which is found only in trace amounts in most plants, has been suggested to function as a signaling molecule that relays information about carbohydrate availability to other signaling pathways (*15*). In agreement with the proposed role of T6P as a central hub in carbon signaling, *TPS1* loss-of-function mutants are embryonic lethal (*16*). Expression of *TPS1* from the seed-specific *ABI3* promoter has been shown to be sufficient to rescue the embryo defect, but the resulting homozygous *tps1 ABI3:TPS1* plants develop slowly and senesce before entering the reproductive phase (*17*). Homozygous *tps1-2* mutants have also been recovered using a chemically inducible rescue construct (*GVG:TPS1*), which enables induction of *TPS1* by dexamethasone application, allowing the *tps1-2 GVG:TPS1* embryos to be rescued to give viable plants that can be stably maintained (*18*). The resulting *tps1-2 GVG:TPS1* plants flower extremely late, producing infertile flowers on shoots that simultaneously arise from the shoot apical meristem (SAM) and axillary meristems, or completely fail to flower, even under inductive photoperiod. These findings indicate that TPS1 plays a critical role in controlling the transition to flowering. However, it is currently unclear where TPS1 is integrated into the canonical flowering-time pathways.

To better understand the molecular function of TPS1, we first confirmed its effect on flowering by knocking down *TPS1* expression with the use of an artificial microRNA (*35S:amiR-TPS1*; figs. S1 and S2) (*19*). This resulted in a significant 25 to 30% reduction in T6P levels (fig. S3) and a delay in flowering by more than 20 leaves (Table 1, experiment 1; fig. S4). In contrast, sucrose levels were significantly higher in *35S:amiR-TPS1* plants (fig. S4), indicating that carbohydrate availability as such was not compromised in those plants. These findings highlight

[1]Department of Metabolic Networks, Max Planck Institute of Molecular Plant Physiology, Am Mühlenberg 1, 14476 Potsdam, Germany. [2]Department of Molecular Biology, Max Planck Institute for Developmental Biology, Spemannstr. 35, 72076 Tübingen, Germany.

*To whom correspondence should be addressed. E-mail: vanessa.wahl@mpimp-golm.mpg.de (V.W.); maschmid@tuebingen.mpg.de (M.S.)

www.sciencemag.org/cgi/content/full/science.1231573/DC1

Supplementary Materials for

53BP1 Regulates DSB Repair Using Rif1 to Control 5′ End Resection

Michal Zimmermann, Francisca Lottersberger,
Sara B. Buonomo, Agnel Sfeir, Titia de Lange*

*To whom correspondence should be addressed. E-mail: delange@mail.rockefeller.edu

Published 10 January 2013 on *Science* Express
DOI: 10.1126/science.1231573

This PDF file includes:

SUPPLEMENTAL ON LINE MATERIALS

SUPPLEMENTARY ACKNOWLEDGEMENT

This work was realized in part in CEITEC - Central European Institute of Technology - with research infrastructure supported by the project CZ.1.05/1.1.00/02.0068, and project CZ.1.07/2.3.00/30.0019 financed from the European Regional Development Fund.

MATERIALS and METHODS

Cell culture and generation of genetically modified MEFs

Rif1$^{F/F}$, TRF2$^{F/F}$, TRF1$^{F/F}$, 53BP1$^{-/-}$, and Lig4$^{-/-}$ mice were described previously (*1-5*). Compound genotypes were obtained by intercrossing and MEFs were isolated from E13.5 or E12.5 (for Lig4$^{-/-}$) embryos using standard techniques. Genotyping was performed by Transnetyx using real-time PCR. Primary MEFs were immortalized at PD 1 or 2 by two consecutive retroviral infections with pBabe-SV40LT (a gift from G. Hannon) and cultured in DMEM (GIBCO) supplemented with 10 or 15% fetal bovine serum (GIBCO), 2 mM L-glutamine, 100 U/ml penicillin (Sigma), 0.1 mg/ml streptomycin (Sigma), 0.1 mM nonessential amino acids (Invitrogen), 1 mM sodium pyruvate (Sigma), and 50 mM β-mercaptoethanol (Chemicon). 293T and Phoenix virus packaging cell lines were grown in DMEM supplemented with 10% bovine calf serum (Hyclone), glutamine, nonessential amino acids and penicillin/streptomycin as above.

Cre-mediated gene deletion

The Cre recombinase was introduced by three consecutive infections with a pMMP Hit&Run Cre retrovirus without subsequent antibiotic selection. 5x10^5 MEFs were plated for infections. Experimental time points were counted starting 12 h after the first infection. Cells were plated for harvest at t = 24 h and harvested at time points indicated in each experiment.

For the TRF2$^{F/-}$ Rosa26 Cre-ER^{T1} inducible cell line, Cre expression was triggered by addition of 1 μM 4OH-tamoxifen (4OHT) to the growth media. Media was exchanged 6 h

after 4OHT addition and this point was used as t = 0 when counting experimental time points.

Retroviral gene delivery

For retroviral infections, 2-3x10^6 Phoenix ecotropic packaging cells (ATCC) were plated ~24 h prior to transfection. These cells were transfected with 20 μg of the desired plasmid using $CaPO_4$ precipitation. Cells were provided with fresh medium twice, at 12-16 and 24-30 h after transfection. 48 h after transfection, virus-containing media were collected, filtered through a 0.45 μm filter, supplemented with 4 μg/ml polybrene and used for infection of target cells (5x10^5 MEFs per 10 cm dish). Media of packaging cells were replenished and the same cells were used for later infections.

For expression of exogenous protein constructs, 2-3 infections in 12 h intervals were applied. 12 h after the last infection, 5x10^5 infected cells were plated in selective media containing appropriate antibiotics (1.5-2 μg/ml puromycin or 90 μg/ml hygromycin). Selection was maintained until all cells in an uninfected control plate were dead (2-3 days for puromycin and 5-7 days for hygromycin).

For transduction of shRNA encoding plasmids, 5-6 infections in 4 h intervals over two days were used. 12 h after the last infection, 5x10^5 cells were plated into selective media. Where desirable, Cre-mediated gene deletion was performed after shRNA infections as described above. The first pMMP Hit&Run Cre infection was applied 48 h after the last shRNA infection.

Immunoblotting

Immunoblotting was performed as described previously (*4*). Cells were collected by trypsinization, lysed in 2x Laemmli buffer (100 mM Tris-HCl pH 6.8, 200 mM DTT, 3% SDS, 20% glycerol, 0.05% bromophenol blue) at a concentration of 1x10^4 cells/μl and heated to 80-90°C in a sand bath for 5 min. The lysate was sheared using an insulin needle and run on an SDS-PAGE gel. An equivalent of 1-2x10^5 cells was loaded per lane. The separated proteins were then blotted on a nitrocellulose membrane, blocked with blocking solution [5% non-fat dry milk (BioRad) in PBS/0.1% Tween 20] for at least 30 min and incubated with primary antibody in blocking solution either at least 1 h at room temperature or overnight at 4°C. The membranes were washed 3x 5 min with PBS/0.1% Tween 20 and incubated with a horseradish peroxidase-conjugated secondary antibody in blocking solution for 1 h at room temperature. Chemiluminescent

detection was performed using an ECL Plus Western Blotting Detection System kit (GE Healthcare) according to the manufacturer's protocol. For antibodies see the section on IF and IF-FISH below.

Live-cell imaging and chromatin mobility measurement

Live-cell imaging was performed essentially as described previously (*10*). Dysfunctional telomeres were visualized using a previously characterized mCherry-53BP1$^{1220\text{-}1711}$ allele. In TRF2$^{F/F}$Rif1$^{F/F}$, TRF2$^{F/F}$Rif1$^{+/+}$ and TRF2$^{F/-}$53BP1$^{-/-}$ cells expressing this allele, Rif1 and/or TRF2 deletion was induced by Cre, the cells were plated on glass-bottom plates (MatTek) and imaged at 66 – 72 h post Cre. The growth medium was exchanged to Leibovitz's 7imaging. Time-lapse movies of the cells were captured using a DeltaVision RT microscope system (Applied Precision) with a PlanApo 360 1.40 n.a. objective lens (Olympus). The system was operated using SoftWoRx software. 5-mm Z-stacks at 0.5 mm steps were acquired every 30 s over 20 min (total 40 frames) at 2x binning and 512 x 512 pixel resolution. The movies were later deconvolved and maximum Z-projections were generated using SoftWorRx software.

Image analysis was conducted in ImageJ software. At first, the image stacks were registered using the StackReg plugin (*11*), with the "scaled rotation" or "affine" settings) and trajectories of the individual TIFs were calculated by the ParticleTracker 3D plugin (*12*). The analysis parameters were set as follows: radius = 2 px; cutoff = 2 px; percentile = 2 - 4; link range = 1; displacement = 5 px. Cumulative traveled distance was calculated for each trajectory as described previously (*10*). At least ten cells were analyzed for each genotype per experiment. All dysfunctional telomeres continuously tracked for at least 35 frames were selected for analysis (on average ~30-40 trajectories per cell).

shRNAs

shRNAs to BLM, CtIP, and Exo1 were previously described (*6*). The targeting sequence of the BRCA1 shRNA was 5' GCAGCGTTCAGAAAGTTAA 3'.

IF and IF-FISH

IF and IF-FISH were performed as described previously (*5, 7*). Cells were grown on coverslips to sub-confluence, washed with PBS and fixed in 3% paraformaldehyde/PBS for 10 min at room temperature. Fixed cells were permeabilized with Triton X-100 buffer (0.1% Triton X-100, 20 mM HEPES-KOH pH 7.9, 50 mM NaCl, 3 mM MgCl2, 300 mM

sucrose) for 5 min and blocked in PBG [0.2% (w/v) cold water fish gelatin (Sigma) and 0.5% (w/v) BSA (Sigma) in PBS] for 30 min at room temperature. Cells were then incubated with primary antibody in PBG for 2 h at room temperature, followed by three 5 min washes with PBS. Fluorescently labeled secondary antibody in PBG was then added for 1 h at room temperature and coverslips were washed 3x with PBS (DAPI was present in second wash) and mounted in ProLong Gold antifade reagent.
When telomeric FISH was to be performed after IF, the coverslips were washed after incubation with the secondary antibody and fixed again in 3% paraformaldehyde/PBS for 5 min followed by two 5 min washes with PBS and dehydration in 70%, 95%, 100% ethanol series. The coverslips were air-dried, a FITC-OO-$[CCCTAA]_3$ PNA probe (Applied Biosystems) in hybridization solution [70% formamide, 0.5% (w/v) blocking reagent (Roche), 10 mM Tris-HCl pH 7.2] was added and DNA on the coverslips was denatured on a 80°C heating block for 3-5 min. Hybridization was performed either for 2 h at room temperature or overnight at 4°C. Coverslips were then washed 2x 15 min with 70% formamide, 10 mM Tris-HCl pH 7.2 and 3x with PBS, and mounted as above.

For Myc-RPA and BARD1 staining, MEFs were infected with a Myc-tagged RPA32 retrovirus as described previously (*8*) and grown on poly-L-lysine coated coverslips (BD Biosciences). Soluble nucleoplasmic proteins were extracted prior to fixation using a published protocol (*9*). Briefly, coverslips were washed twice with cold PBS, treated with cold cytoskeleton buffer (10 mM PIPES pH 6.8, 100 mM NaCl, 300 mM sucrose, 3 mM $MgCl_2$, 1 mM EGTA, 0.5% Triton X-100) for 5 min and then 5 min with cold cytoskeleton stripping buffer (10 mM Tris-HCl pH 7.4, 10 mM NaCl, 3 mM $MgCl_2$, 1% Tween 20, 0.5% Na^+-deoxycholate). The cells were then washed 3x with cold PBS. All steps were performed on ice. Extracted cells on coverslips were then fixed with 3% paraformaldehyde, 2% sucrose in PBS (10 min, room temperature) and processed for IF as described above.

For BrdU staining, coverslips were treated with 4N HCl for 4 min at room temperature to denature DNA prior to incubation with antibodies.
Images were captured using a Zeiss Axioplan II microscope equipped with a Hamamatsu C4742-95 camera and controlled by OpenLab software (Improvision).

The following primary antibodies were used for immunoblotting and immunofluorescence: Rabbit anti-Rif1 (1240), rabbit anti-TRF2 (1254), rabbit anti-TRF1 (1449), rabbit anti-53BP1 (for IF: NB100-304; for IB: NB100-305; both Novus Biologicals), rabbit anti-CtIP (H-300, Santa Cruz), rabbit anti-BLM (Ab2179, Abcam),

rabbit anti-BARD1 (H-300, Santa Cruz), rabbit anti-γ-H2AX (20E3, Cell Signalling), mouse anti-γ-H2AX (JBW301, Millipore), mouse anti-Myc (9B11, Cell Signaling), mouse anti-Chk2 (BD Biosciences), mouse anti-BrdU (BD Biosciences), mouse anti-γ-tubulin (GTU-88, Sigma).

Telomere overhang analysis by in-gel hybridization

In gel assays to determine changes in the amount of single-stranded telomeric DNA were performed as described previously (*4*). 0.5 - 1x10^6 cells were harvested by trypsinization, re-suspended in PBS, mixed 1:1 with 2% agarose in PBS and cast into plugs. The plugs were then digested overnight at 50°C with 1 mg/ml Proteinase K (Roche) in 10 mM Tris-HCl pH 8.0, 250 mM EDTA, 0.2% sodium deoxycholate and 1% sodium lauryl sarcosine. The next day, the plugs were washed five times for 1 h each with TE (1 mM PMSF was added to the fourth wash) and once with sterile water (20 min). DNA in the plugs was subsequently digested by *Alu*I and *Mbo*I (NEB; 60 U of each per plug, in NEB Buffer 4) overnight at 37°C. The next morning, plugs were washed once with TE and equilibrated with 0.5x TBE. The samples were loaded onto a 1% agarose in 0.5x TBE gel and run on a CHEF-DRII pulse field electrophoresis apparatus (BioRad). The electrophoresis parameters were as follows: Initial pulse: 5 s, final pulse: 5 s, voltage: 6 V/cm, run time: 24 h. The gel was then dried and pre-hybridized with Church mix for 1 h at 50°C. DNA in the gel was hybridized overnight at 50°C in Church mix with 50 ng of ^{32}P end-labeled $[AACCCT]_4$ probe. After hybridization, the gel was washed three times 30 min with 4x SSC at 55°C, once with 4xSSC/0.1% SDS and exposed to a phosphoimager screen overnight or longer. After exposure, the screen was scanned on a STORM phosphoimager (Molecular Dynamics) and the gel was denatured in 0.5 M NaOH, 1.5 M NaCl for 30 min, neutralized twice (15 min each) with 0.5 M Tris-HCl pH 7.5, 3 M NaCl, pre-hybridized in Church mix for 1 h at 55°C and hybridized overnight with the same probe as above at 55°C. The next day the gel was washed and exposed as above. The ssDNA and dsDNA signals were quantified with ImageQuant software (Molecular Dynamics). The telomeric 3' overhang signal is quantified based on the signal obtained after annealing a labeled C-strand telomeric oligonucleotide to native telomeric DNA and these signals are normalized to the total telomeric DNA signals in each lane obtained after in situ denaturation of the DNA and re-hybridization with the same probe. The normalized signals are then compared between samples to determine

the effect of genotypes or treatments on the relative normalized 3' overhang signals. Data are derived from at least three independent experiments.

Analysis of telomeres by Chromosome Orientation (CO)-FISH

CO-FISH was performed as previously described (*4*). Sub-confluent cells were labeled by 10 μM BrdU:BrdC (3:1) 12 h prior to harvest. 1 h before the indicated harvesting time points, 0.2 μg/ml colcemid was added to the media and cells were later harvested by trypsinization, washed once with PBS, incubated with 0.075 M KCl at 37°C for 10 min and fixed overnight in methanol:acetic acid (3:1). Subsequently, metaphase spreads were dropped onto glass slides in a Thermotron cycler (20°C, 50% humidity) and air-dried overnight. The next day, slides were re-hydrated with PBS, treated with 0.5 mg/ml RNase A (in PBS, 10 min, 37°C), stained with 0.5 μg/ml Hoechst 33258 (Sigma) in 2x SSC for 15 min and exposed to 365-nm UV light (Stratalinker 1800 UV irradiator) for 30 min. The pyrimidine analog-substituted DNA strands were then degraded with Exonuclease III (Promega, 2 x 800 U at room temperature, 10 min each, in a buffer supplied by the manufacturer), slides were washed 3x with PBS, dehydrated in 70%, 95% and 100% ethanol series (5 min each) and air-dried. Slides were then hybridized with a Tamra-OO-$[TTAGGG]_3$ PNA probe (Applied Biosystems) in 70% formamide, 1 mg/ml blocking reagent (Roche) and 10 mM TrisHCl pH 7.2 for 2 h at room temperature. After the first hybridization, slides were rinsed in 70% formamide/10 mM Tris-HCl pH 7.2 and hybridized with a FITC-OO-$[CCCTAA]_3$ PNA probe (same hybridization conditions as above). Slides were then washed 2x 15 min with 70% formamide/10 mM Tris-HCl pH 7.2 and 3x5 min with 0.1 M Tris-HCl pH 7.0/0.15 M NaCl/0.08% Tween-20. 1 μg/ml 4,6-diamidino-2-phenylindole (DAPI) was added to the second of the three washes. After washing, slides were dehydrated as above, air-dried and mounted in ProLong Gold antifade reagent (Invitrogen). Images were captured using a Zeiss Axioplan II microscope equipped with a Hamamatsu C4742-95 camera and controlled by OpenLab software (Improvision).

Induction of DSBs

DSBs were induced by adding 100 μg/ml zeocin (Invitrogen) to the media for 1 h. The drug was subsequently washed out and fresh media was added to the cells. The cells were incubated for an additional hour to allow DSB processing and then fixed and immunostained as described below.

PARPi treatment and assay for mis-rejoined chromosomes

Cells were grown with or without 5 μM Olaparib PARPi (AZD2281, Selleck Chemicals) for 24 h and metaphases were harvested and dropped on microscope slides as described for CO-FISH. After the slides had dried overnight, they were re-hydrated in PBS, stained with 0.25 μg/ml DAPI, dehydrated in 70%, 95%, 100% ethanol series, mounted, and imaged as described for CO-FISH. The lesions were scored as a percentage of chromosomes fused into mis-rejoined chromosomal structures (i.e. number of centromeres in the aberrant structures) compared to total number of chromosomes.

SUPPLEMENTARY REFERENCES

1. A. Sfeir *et al.*, *Cell* **138**, 90 (2009).
2. I. M. Ward, K. Minn, J. van Deursen, J. Chen, *Mol Cell Biol* **23**, 2556 (2003).
3. K. M. Frank *et al.*, *Nature* **396**, 173 (1998).
4. G. B. Celli, T. de Lange, *Nat Cell Biol* **7**, 712 (2005).
5. S. Buonomo, Y. Wu, D. Ferguson, T. de Lange, *J Cell Biol* **187**, 385 (2009).
6. A. Sfeir, T. de Lange, *Science* **336**, 593 (2012).
7. H. Takai, A. Smogorzewska, T. de Lange, *Curr Biol* **13**, 1549 (2003).
8. Y. Gong, T. de Lange, *Mol Cell* **40**, 377 (2010).
9. O. K. Mirzoeva, J. H. Petrini, *Mol Cell Biol* **21**, 281 (2001).
10. N. Dimitrova, Y. C. Chen, D. L. Spector, T. de Lange, *Nature* **456**, 524 (2008).
11. P. Thevenaz, U. E. Ruttimann, M. Unser, *IEEE Trans Image Process* **7**, 27 (1998).
12. I. F. Sbalzarini, P. Koumoutsakos, *J Struct Biol* **151**, 182 (2005).

SUPPLEMENTAL FIGURES AND FIGURE LEGENDS

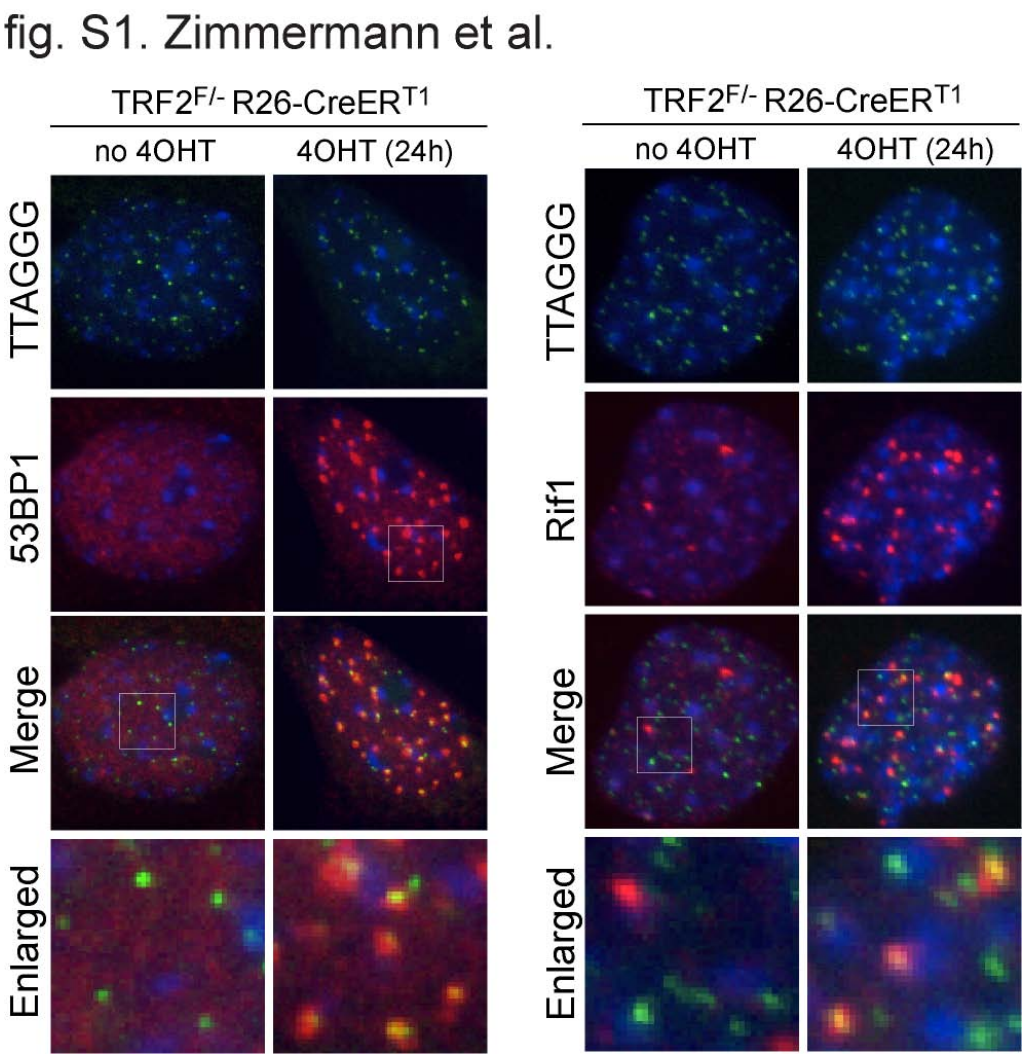

fig. S1 (related to Fig.1). Control showing localization of Rif1 to TRF2-depleted telomeres in the presence of endogenous 53BP1. Representative IF images of TRF2$^{F/-}$Rosa26 CreER^{T1} MEFs showing localization of 53BP1 and Rif1 to dysfunctional telomeres. TRF2 was deleted by 4OH-tamoxifen (4OHT) and localization of 53BP1 (left) and Rif1 (right) was visualized by IF (red) along with a telomeric TTAGGG FISH (green). DNA was counterstained with DAPI (blue). Note similarity of Rif1 localization to dysfunctional telomeres in the presence of endogenous wild type 53BP1 and the 53BP1^{DB} allele shown in Figure 1.

fig. S2. Zimmermann et al.

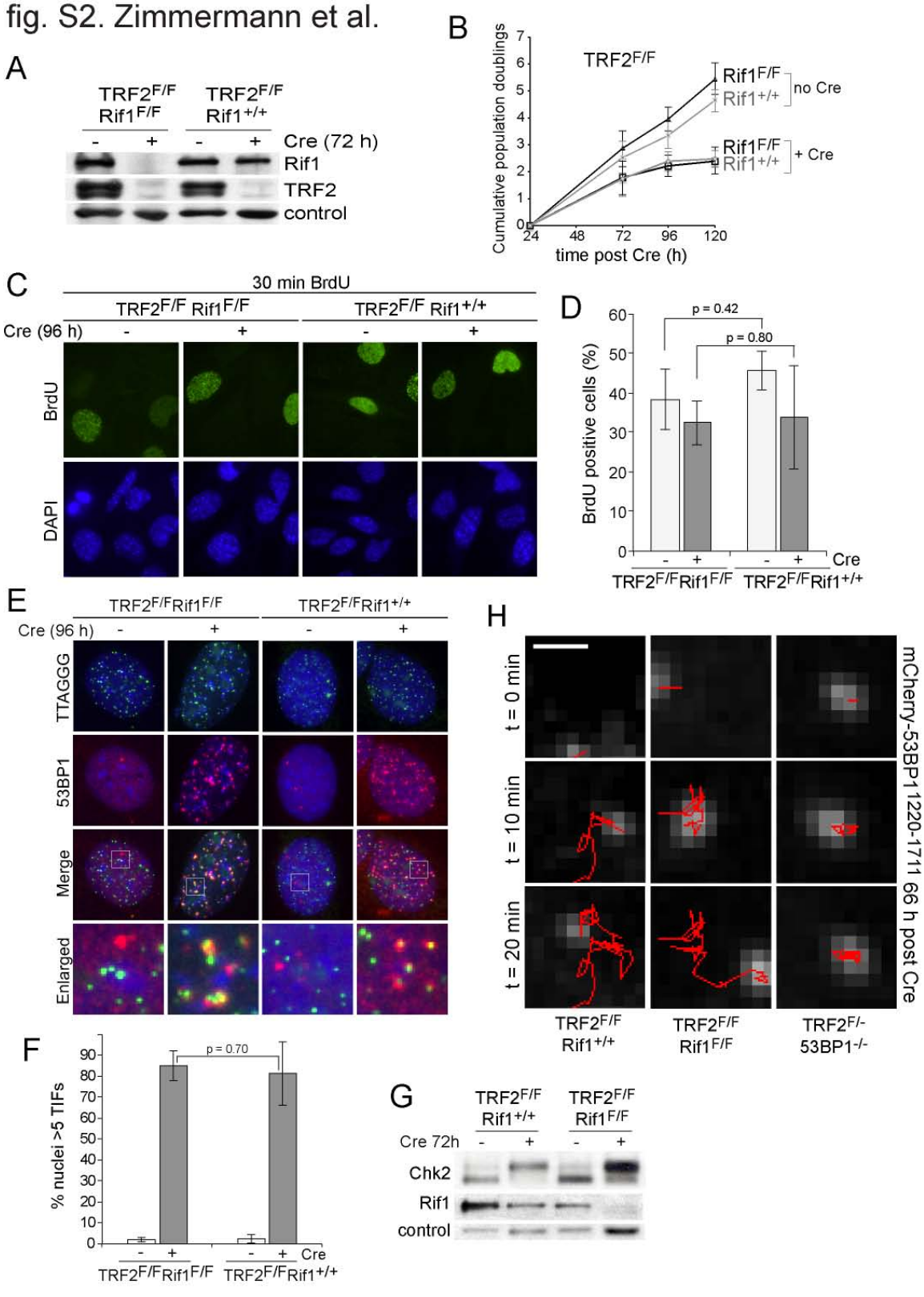

fig. S2 (related to Fig. 2). (A) Immunoblots showing deletion of Rif1 and/or TRF2 in SV40-LT immortalized TRF2$^{F/F}$Rif1$^{F/F}$ and TRF2$^{F/F}$Rif1$^{+/+}$ MEFs 72 h after Cre. (B) Proliferation of the cells shown in (A). (C) IF images of TRF2$^{F/F}$Rif1$^{+/+}$ and TRF2$^{F/F}$Rif1$^{F/F}$ MEFs showing cells in S-phase. Cells were labeled with 10 μM BrdU for 30 min, fixed and processed for denaturing BrdU IF (green) as described in materials and methods. DAPI staining is visualized in blue. (D) Graph showing quantification of BrdU positive cells in experiments shown in (C). (E) IF images of TRF2$^{F/F}$Rif1$^{+/+}$ and TRF2$^{F/F}$Rif1$^{F/F}$ MEFs showing localization of 53BP1 (red) to telomeres lacking TRF2 irrespective of Rif1 status. Telomeric TTAGGG FISH is shown in green; DAPI-stained DNA is in blue. (F) Graph showing quantification of 53BP1 containing TIFs as shown in (E). Data in (D) and (F) are means of three independent experiments ±SDs. P values were calculated using a two-tailed paired Student's t-test. (G) Immunoblotting showing phosphorylation of Chk2 in TRF2- and Rif1-deleted cells (72 h after Cre). (H) Examples of traces of mCherry-53BP1$^{1220\text{-}1711}$ in the indicated MEFs during a 20 min live-cell time-lapse imaging experiment. Examples of fast moving foci are shown on the left and in the middle and a slowly moving focus is shown at right.

fig. S3. Zimmermann et al.

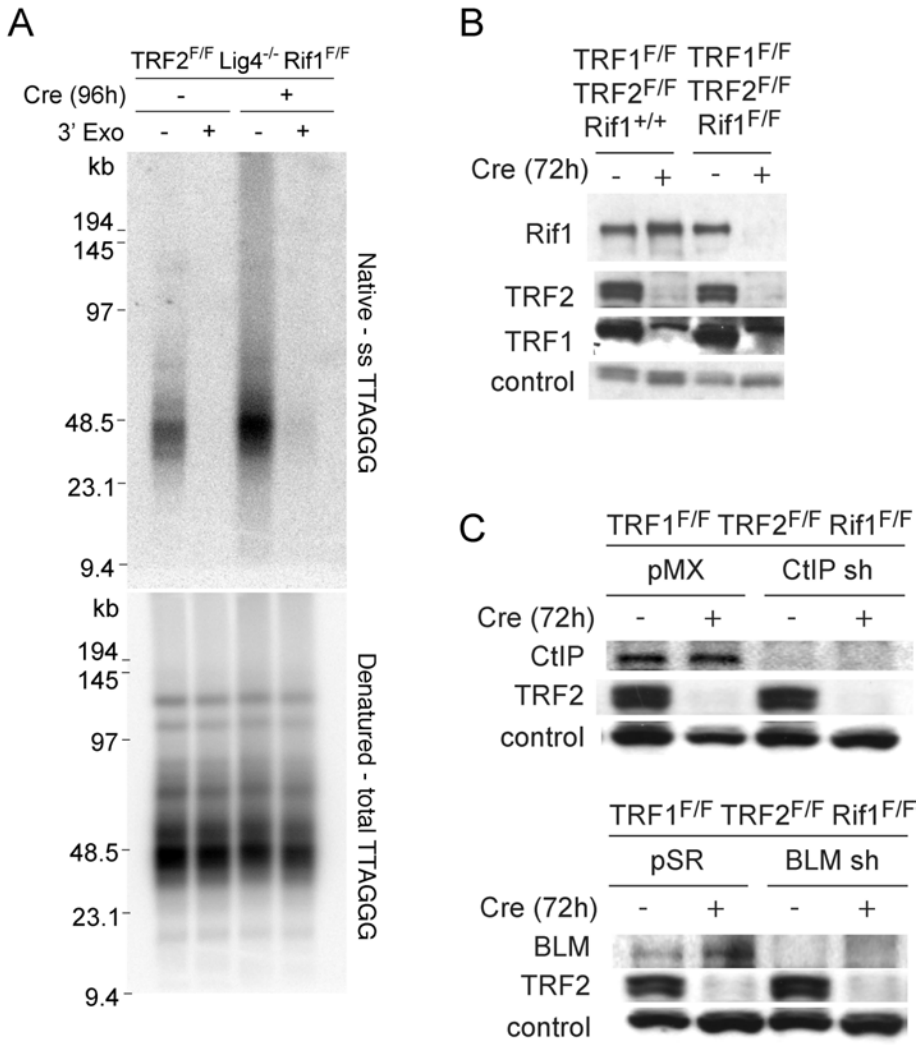

fig. S3 (related to Fig. 3). (A) Immunoblots showing Cre-mediated deletion of Rif1 and shelterin components TRF1 and TRF2 in SV40-LT immortalized TRF1$^{F/F}$TRF2$^{F/F}$Rif1$^{+/+}$ and TRF1$^{F/F}$TRF2$^{F/F}$Rif1$^{F/F}$ MEFs. Cells were harvested 72 h after Cre induction. (B) Immunoblots showing depletion of CtIP and BLM in TRF1$^{F/F}$TRF2$^{F/F}$Rif1$^{F/F}$ cells by shRNA. ShRNA expressing retroviruses were delivered by 4-5 infections and the targeted genes were subsequently deleted by the Cre recombinase. Cells were processed 96 h after Cre induction, corresponding to 180 h after the first introduction of the shRNAs.

fig. S4. Zimmermann et al.

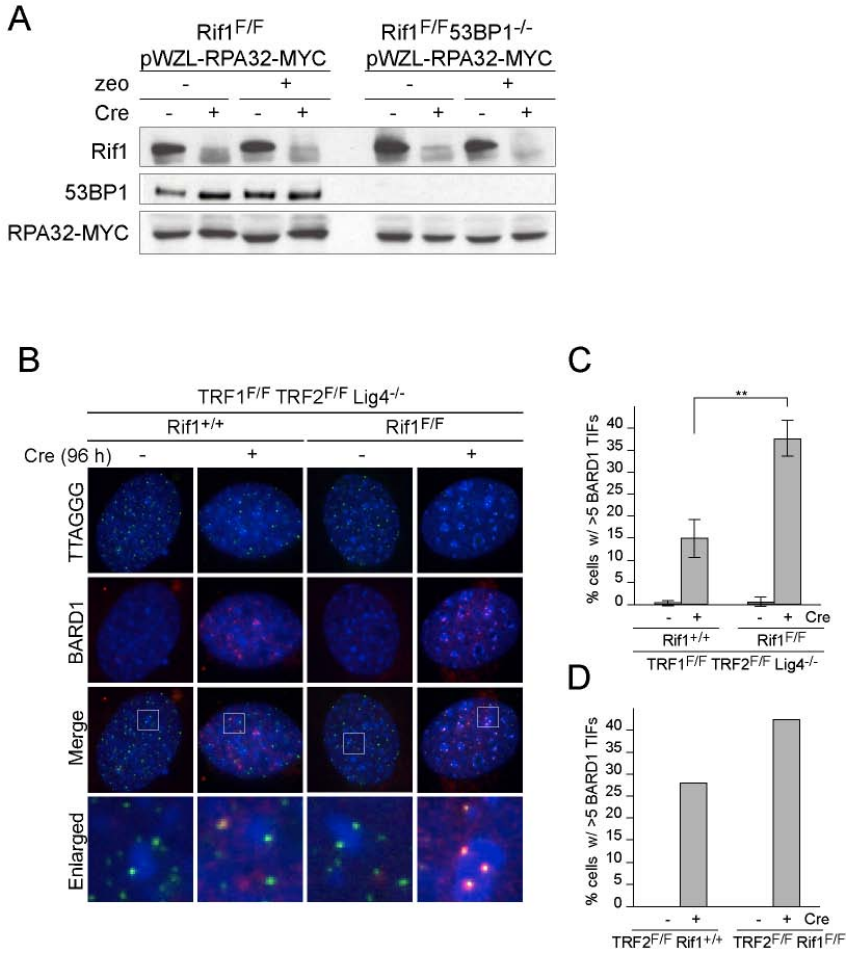

fig. S4 (related to Fig. 4). (A) Immunoblots showing expression of exogenous MYC-RPA32 protein in SV40-LT immortalized Rif1$^{F/F}$ and Rif1$^{F/F}$53BP1$^{-/-}$ MEFs, and deletion of Rif1 96 h after Cre induction. (B) IF images showing accumulation of BARD1 at dysfunctional telomeres devoid of all shelterin components. TRF1$^{F/F}$TRF2$^{F/F}$Lig4$^{-/-}$Rif1$^{F/F}$ MEFs were treated with Cre, and BARD1 was visualized by immunofluorescence (red). Telomeric TTAGGG FISH is shown in green, DNA was stained by DAPI (blue). (C) Graph showing percentage of cells displaying >5 BARD1-telomere colocalizations as shown in (B). Means of three independent experiments ±SDs. P value was calculated using a two-tailed Student's t-test. (D) Percentage of nuclei showing >5 BARD1-positive TIFs in TRF2$^{F/F}$Rif1$^{+/+}$ and TRF2$^{F/F}$Rif1$^{F/F}$ MEFs. Data from one representative experiment.

Full Reference List

1. A. T. Noon, A. A. Goodarzi, 53BP1-mediated DNA double strand break repair: insert bad pun here. *DNA Repair* **10**, 1071 (2011). doi:10.1016/j.dnarep.2011.07.012 Medline

2. I. M. Ward, K. Minn, J. van Deursen, J. Chen, p53 Binding protein 53BP1 is required for DNA damage responses and tumor suppression in mice. *Mol. Cell. Biol.* **23**, 2556 (2003). doi:10.1128/MCB.23.7.2556-2563.2003 Medline

3. J. C. Morales *et al*., Role for the BRCA1 C-terminal repeats (BRCT) protein 53BP1 in maintaining genomic stability. *J. Biol. Chem.* **278**, 14971 (2003). doi:10.1074/jbc.M212484200 Medline

4. S. Difilippantonio *et al*., 53BP1 facilitates long-range DNA end-joining during V(D)J recombination. *Nature* **456**, 529 (2008). doi:10.1038/nature07476 Medline

5. N. Dimitrova, Y. C. Chen, D. L. Spector, T. de Lange, 53BP1 promotes non-homologous end joining of telomeres by increasing chromatin mobility. *Nature* **456**, 524 (2008). doi:10.1038/nature07433 Medline

6. S. F. Bunting *et al*., 53BP1 inhibits homologous recombination in Brca1-deficient cells by blocking resection of DNA breaks. *Cell* **141**, 243 (2010). doi:10.1016/j.cell.2010.03.012 Medline

7. A. Bothmer *et al*., Regulation of DNA end joining, resection, and immunoglobulin class switch recombination by 53BP1. *Mol. Cell* **42**, 319 (2011). doi:10.1016/j.molcel.2011.03.019 Medline

8. A. Sfeir, T. de Lange, Removal of shelterin reveals the telomere end-protection problem. *Science* **336**, 593 (2012). doi:10.1126/science.1218498 Medline

9. L. Xu, E. H. Blackburn, Human Rif1 protein binds aberrant telomeres and aligns along anaphase midzone microtubules. *J. Cell Biol.* **167**, 819 (2004). doi:10.1083/jcb.200408181 Medline

10. J. Silverman, H. Takai, S. B. Buonomo, F. Eisenhaber, T. de Lange, Human Rif1, ortholog of a yeast telomeric protein, is regulated by ATM and 53BP1 and functions in the S-phase checkpoint. *Genes Dev.* **18**, 2108 (2004). doi:10.1101/gad.1216004 Medline

11. M. S. Huen *et al*., Regulation of chromatin architecture by the PWWP domain-containing DNA damage-responsive factor EXPAND1/MUM1. *Mol. Cell* **37**, 854 (2010). doi:10.1016/j.molcel.2009.12.040 Medline

12. C. F. Hardy, L. Sussel, D. Shore, A RAP1-interacting protein involved in transcriptional silencing and telomere length regulation. *Genes Dev.* **6**, 801 (1992). doi:10.1101/gad.6.5.801 Medline

13. S. Anbalagan, D. Bonetti, G. Lucchini, M. P. Longhese, Rif1 supports the function of the CST complex in yeast telomere capping. *PLoS Genet.* **7**, e1002024 (2011). doi:10.1371/journal.pgen.1002024 Medline

14. D. Bonetti *et al*., Shelterin-like proteins and Yku inhibit nucleolytic processing of *Saccharomyces cerevisiae* telomeres. *PLoS Genet.* **6**, e1000966 (2010). doi:10.1371/journal.pgen.1000966 Medline

15. S. B. Buonomo, Y. Wu, D. Ferguson, T. de Lange, Mammalian Rif1 contributes to replication stress survival and homology-directed repair. *J. Cell Biol.* **187**, 385 (2009). doi:10.1083/jcb.200902039 Medline

16. D. Cornacchia *et al*., Mouse Rif1 is a key regulator of the replication-timing programme in mammalian cells. *EMBO J.* **31**, 3678 (2012). doi:10.1038/emboj.2012.214 Medline

17. S. Yamazaki *et al*., Rif1 regulates the replication timing domains on the human genome. *EMBO J.* **31**, 3667 (2012). doi:10.1038/emboj.2012.180 Medline

18. A. A. Sartori *et al*., Human CtIP promotes DNA end resection. *Nature* **450**, 509 (2007). doi:10.1038/nature06337 Medline

19. X. Yu, L. C. Wu, A. M. Bowcock, A. Aronheim, R. Baer, The C-terminal (BRCT) domains of BRCA1 interact in vivo with CtIP, a protein implicated in the CtBP pathway of transcriptional repression. *J. Biol. Chem.* **273**, 25388 (1998). doi:10.1074/jbc.273.39.25388 Medline

20. A. K. Wong *et al*., Characterization of a carboxy-terminal BRCA1 interacting protein. *Oncogene* **17**, 2279 (1998). doi:10.1038/sj.onc.1202150 Medline

21. H. Takai, A. Smogorzewska, T. de Lange, DNA damage foci at dysfunctional telomeres. *Curr. Biol.* **13**, 1549 (2003). doi:10.1016/S0960-9822(03)00542-6 Medline

22. A. Sfeir *et al*., Mammalian telomeres resemble fragile sites and require TRF1 for efficient replication. *Cell* **138**, 90 (2009). doi:10.1016/j.cell.2009.06.021 Medline

23. K. M. Frank *et al*., Late embryonic lethality and impaired V(D)J recombination in mice lacking DNA ligase IV. *Nature* **396**, 173 (1998). doi:10.1038/24172 Medline

24. G. B. Celli, T. de Lange, DNA processing is not required for ATM-mediated telomere damage response after TRF2 deletion. *Nat. Cell Biol.* **7**, 712 (2005). doi:10.1038/ncb1275 Medline

25. Y. Gong, T. de Lange, A Shld1-controlled POT1a provides support for repression of ATR signaling at telomeres through RPA exclusion. *Mol. Cell* **40**, 377 (2010). doi:10.1016/j.molcel.2010.10.016 Medline

26. O. K. Mirzoeva, J. H. Petrini, DNA damage-dependent nuclear dynamics of the Mre11 complex. *Mol. Cell. Biol.* **21**, 281 (2001). doi:10.1128/MCB.21.1.281-288.2001 Medline

27. P. Thévenaz, U. E. Ruttimann, M. Unser, A pyramid approach to subpixel registration based on intensity. *IEEE Trans. Image Process.* **7**, 27 (1998). doi:10.1109/83.650848 Medline

28. I. F. Sbalzarini, P. Koumoutsakos, Feature point tracking and trajectory analysis for video imaging in cell biology. *J. Struct. Biol.* **151**, 182 (2005). doi:10.1016/j.jsb.2005.06.002 Medline